ACES Asian Chemical Editorial Society

DOI: 10.1002/asia.202000009

CHEMISTRY AN ASIAN JOURNAL Full Paper

How Alkali Cations Catalyze Aromatic Diels-Alder Reactions

Pascal Vermeeren,[a] Francine Brinkhuis,[a] Trevor A. Hamlin,*[a] and F. Matthias Bickelhaupt*[a, b]

Abstract: We have quantum chemically studied alkali cation-catalyzed aromatic Diels-Alder reactions between benzene and acetylene forming barrelene using relativistic, dispersion-corrected density functional theory. The alkali cation-catalyzed aromatic Diels-Alder reactions are accelerated by up to 5 orders of magnitude relative to the uncatalyzed reaction and the reaction barrier increases along the series $Li^+ < Na^+ < K^+ < Rb^+ < Cs^+ <$ none. Our detailed activation strain and molecular-orbital bonding analyses reveal that the alkali cations lower the aromatic Diels-Alder reaction barrier by reducing the Pauli repulsion between the closed-shell filled orbitals of the dienophile and the aromatic diene. We argue that such Pauli mechanism behind Lewis-acid catalysis is a more general phenomenon. Also, our results may be of direct importance for a more complete understanding of the network of competing mechanisms towards the formation of polycyclic aromatic hydrocarbons (PAHs) in an astrochemical context.

Introduction

Aromatic Diels-Alder (DA) reactions involve the [4+2] cycloaddition between an aromatic diene and a dienophile and are extremely slow or not allowed due to the aromatic nature of the diene.[1] Kinetic studies, for example, have shown that aromatic dienes, such as polycyclic aromatic hydrocarbon (PAHs) do not react with maleic anhydride under mild conditions.[2] The DA reactivity of aromatic systems can be significantly enhanced by the introduction of Lewis acids or by geometrical predistortion of the aromatic diene.[3,4] It is generally understood that the strong donor-acceptor interaction between a Lewis acid and one of the reactants, e.g., the aromatic diene, results in a significant stabilization of the LUMO of that respective reactant, which, in turn, leads to a smaller HOMO–LUMO orbital energy gap and, consequently, to a lower reaction barrier compared to an uncatalyzed DA reaction.[5] Recently, we have shown that, in contrast to this current rationale, Lewis acids do not catalyze organic reactions, such as Michael addition or Diels-Alder reactions, by lowering the HOMO–LUMO gap, but instead by reducing the Pauli repulsion, i.e., two-center four-electron repulsion, between the closed-shell filled orbitals of both the reactants.[6] To ascertain the generality of the new electronic mechanism behind Lewis acid-catalyzed organic reactions, we now investigate the catalytic effect of Lewis acidic alkali cations ($\mathbf{M^+}$ = none, Li^+, Na^+, K^+, Rb^+, Cs^+) on the archetypal aromatic Diels-Alder reaction between benzene (**bz**) and acetylene (**yne**), acting as an aromatic diene and dienophile, respectively, forming the bicyclic cycloadduct barrelene (**bl**). Alkali cations exhibit Lewis-acidic catalytic activity on various chemical reactions,[7] and, thus, may serve as potential candidates for catalyzing aromatic DA reactions.

Our computations have been performed using relativistic dispersion-corrected density functional theory (DFT) at ZORA-BLYP-D3(BJ)/TZ2P level,[8–11] as implemented in the Amsterdam Density Functional (ADF) program.[12] The catalytic effect of the alkali cations have been analyzed using the activation strain model (ASM)[13] in conjunction with quantitative Kohn-Sham molecular orbital theory (KS-MO) and a matching canonical energy decomposition analysis (EDA).[14] First, we examine the complexation between the alkali cation and benzene leading to the activated reactant **bz-M$^+$**. Second, we investigate which reaction pathway is the most favorable: acetylene approaching benzene at the side opposite to where the alkali cation is coordinating (opposite-side attack; see Scheme 1) or acetylene

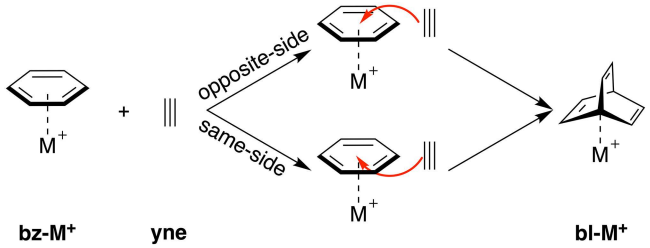

Scheme 1. Opposite-side and same-side alkali cation-catalyzed Diels-Alder reaction of benzene-**M$^+$** (**bz-M$^+$**) with acetylene (**yne**) resulting in the identical cycloadduct barrelene–**M$^+$** (**bl-M$^+$**), where **M$^+$** = none, Li^+, Na^+, K^+, Rb^+, Cs^+.

[a] P. Vermeeren, F. Brinkhuis, Dr. T. A. Hamlin, Prof. Dr. F. M. Bickelhaupt
Department of Theoretical Chemistry
Amsterdam Institute of Molecular and Life Sciences (AIMMS)
Amsterdam Center for Multiscale Modeling (ACMM)
Vrije Universiteit Amsterdam
De Boelelaan 1083, 1081 HV Amsterdam (The Netherlands)
E-mail: t.a.hamlin@vu.nl
f.m.bickelhaupt@vu.nl

[b] Prof. Dr. F. M. Bickelhaupt
Institute for Molecules and Materials
Radboud University Nijmegen
Heyendaalseweg 135, 6525 AJ Nijmegen (The Netherlands)

Supporting information for this article is available on the WWW under https://doi.org/10.1002/asia.202000009

approaching benzene at the same side as where the alkali cation is coordinating (same-side attack). Third, we analyze the catalytic effect of the Lewis acidic alkali cation on the DA reactivity of benzene with acetylene. Finally, to explore how far the barrier of the aromatic DA reaction can be lowered, we combine our findings with insights from the seminal work of Narsaria *et al.*, who studied the effect of predistortion as well as the introduction of heteroatoms on the DA reactivity of benzene.[4b]

Besides serving as a general guide for the development of new approaches to activate aromatic reactants towards aromatic DA reactions, our results are also relevant in an astrochemical context. Polycyclic aromatic hydrocarbons (PAHs) are one of the major classes of carbon-bearing molecules in astrophysical environments,[15] including meteorites, molecular clouds in deep space, interstellar grains, and interplanetary dust particles,[16] carrying up to 20% of all the cosmic elemental carbon.[15b] Despite their prevalence, the mechanism behind the formation of interstellar PAHs is not yet completely understood. Barrelene, the bicyclic product of an aromatic DA reaction between benzene and acetylene, is a key intermediate for the synthesis of PAHs in the laboratory,[17] which makes this reaction pathway a plausible candidate to consider for the formation of PAHs in outer space. Furthermore, the cosmic abundance of alkali cations in various astrophysical environments has been spectroscopically confirmed,[18] which constitutes further support for the idea that the alkali cation-promoted aromatic DA reactions studies herein might occur in outer space.

Computational Method

Computational details

All calculations were performed using the Amsterdam Density Functional (ADF) software package.[12] The GGA exchange-correlation functional BLYP[9a,b] with the finite damping introduced by Becke and Johnson (BJ), BLYP-D3(BJ),[9c,d] was used for the optimizations of all stationary points as well as for the analyses along the reaction coordinate using the activation strain model (ASM)[13] and energy decomposition analysis (EDA).[14] Introducing BJ damping leads to an improvement over DFT-D3 in calculated reaction barriers and energies.[10] Furthermore, Hamlin et al. demonstrated that the BLYP-D3 should be used for studying cycloadditions featuring non-covalent interactions.[19] Scalar relativistic effects are accounted for using the zeroth-order regular approximation (ZORA).[8] The basis set used, denoted TZ2P, is of triple-ζ quality for all atoms and has been improved by two sets of polarization functions.[11] The accuracies of the fit scheme (Zlm fit)[20a] and the integration grid (Becke grid)[20b] were set to VERYGOOD. Geometries were optimized without any symmetry constraint. All calculated stationary points have been verified, through vibrational analysis,[21] to be energy minima (zero imaginary frequencies) or transition states (one imaginary frequency). The character of the normal mode associated with the imaginary frequency of the transition state has been analyzed to ensure it is associated with the reaction of interest. The potential energy surfaces of the studied aromatic Diels-Alder reactions were obtained by performing intrinsic reaction coordinate (IRC) calculations.[22] The obtained potential energy surfaces are analyzed using the PyFrag program.[23] Optimized structures were illustrated using CYLview.[24]

Activation Strain Model and Energy Decomposition Analysis

The activation strain model of chemical reactivity[13] (ASM, also known as the distortion/interaction model[25]), is a fragment-based approach based on the idea that the energy of a reacting system, i.e., the potential energy surface, is described with respect to, and understood in terms of the characteristics of, the original reactants. It considers their rigidity and the extent to which the reactants must deform during the reaction plus their capability to interact as the reaction proceeds. This procedure has shown to be crucial for unraveling the underlying mechanisms in many organic and inorganic reactions.[4b,6,19,26] In this model, we decompose the total energy, $\Delta E(\zeta)$, into the respective total strain and interaction energy, $\Delta E_{strain}(\zeta)$ and $\Delta E_{int}(\zeta)$, and project these values onto the reaction coordinate ζ [Eq. (1)].

$$\Delta E(\zeta) = \Delta E_{strain}(\zeta) + \Delta E_{int}(\zeta) \quad (1)$$

In this equation, the total strain energy, $\Delta E_{strain}(\zeta)$, is the penalty that needs to be paid to deform the reactants from their equilibrium structure to the geometry they adopt during the reaction at point ζ of the reaction coordinate. On the other hand, the interaction energy, $\Delta E_{int}(\zeta)$, accounts for all the chemical interactions that occur between the deformed fragments along the reaction coordinate. The total strain energy can, in turn, be further decomposed into the strain energies corresponding to the deformation of the aromatic diene, $\Delta E_{strain,\mathbf{bz\text{-}M}+}(\zeta)$, as well as from the dienophile, $\Delta E_{strain,\mathbf{yne}}(\zeta)$ [Eq. (2)].

$$\Delta E_{strain}(\zeta) = \Delta E_{strain,\mathbf{bz\text{-}M}+}(\zeta) + \Delta E_{strain,\mathbf{yne}}(\zeta) \quad (2)$$

The interaction energy between the deformed reactants is further analyzed in terms of quantitative Kohn-Sham molecular orbital theory (KS-MO) in combination with a canonical energy decomposition analysis (EDA).[14] The EDA decomposes the $\Delta E_{int}(\zeta)$ into the following four physically meaningful energy terms [Eq. (3)]:

$$\Delta E_{int}(\zeta) = \Delta V_{elstat}(\zeta) + \Delta E_{Pauli}(\zeta) + \Delta E_{oi}(\zeta) + \Delta E_{disp}(\zeta) \quad (3)$$

Herein, $\Delta V_{elstat}(\zeta)$ is the classical electrostatic interaction between the unperturbed charge distributions of the (deformed) reactants and is usually attractive. The Pauli repulsion, $\Delta E_{Pauli}(\zeta)$, comprises the destabilizing interaction between occupied closed-shell orbitals of both fragments due to the Pauli principle. The orbital interaction energy, $\Delta E_{oi}(\zeta)$, accounts for polarization and charge transfer between the fragments,

Table 1. Energy decomposition analysis (in [kcal mol^{-1}]) and **bz**···$\mathbf{M^+}$ distance (in [Å]) between benzene and alkali cation in the reactant **bz**-$\mathbf{M^+}$.[a]

M^+	ΔE	ΔE_{strain}	ΔE_{int}	ΔV_{elstat}	ΔE_{Pauli}	ΔE_{oi}	ΔE_{disp}	r(bz···M^+)[b]
Cs^+	−12.9	0.2	−13.1	−6.8	3.0	−5.9	−3.3	3.941
Rb^+	−15.4	0.2	−15.6	−8.0	3.5	−7.6	−3.5	3.655
K^+	−17.3	0.2	−17.5	−8.8	3.6	−8.9	−3.4	3.453
Na^+	−24.7	0.2	−24.9	−11.2	3.6	−13.8	−3.5	2.977
Li^+	−38.0	0.2	−38.2	−13.0	10.3	−34.3	−1.3	2.317

[a] Computed at ZORA-BLYP-D3(BJ)/TZ2P. [b] Average distance between the alkali cation and all six carbon atoms.

such as HOMO–LUMO interactions. Finally, the dispersion energy, $\Delta E_{disp}(\zeta)$, accounts for the dispersion corrections as introduced by Grimme et al.[10] A detailed, step-by-step, guide on how to perform and interpret the ASM and EDA can be found in reference 13a.

In both the activation strain diagrams and accompanied energy decomposition plots in this study, the energy terms are projected onto the average distance of the two newly forming C···C bonds between the aromatic diene and the dienophile. This critical reaction coordinate undergoes a well-defined change during the reaction from the reactant complex via the transition state to the cycloadduct and is shown to be a valid reaction coordinate for studying cycloadditions.[4b,26c]

Table 2. Reaction barriers $\Delta E^{\ddagger}$, reaction energies ΔE_{rxn} (in [kcal mol^{-1}]), and average length r (in [Å]) of the two newly forming C···C bonds in the transition state for the uncatalyzed and alkali cation-catalyzed Diels-Alder reactions between **bz**-$\mathbf{M^+}$ and **yne**.[a]

M^+	Dienophile Attack	$\Delta E^{\ddagger}$	ΔE_{rxn}	r(C···C)[b]
none	n/a	37.2	7.0	2.106
Cs^+	same-side	36.5	6.2	2.105
	opposite-side	34.3	6.2	2.113
Rb^+	same-side	37.2	5.9	2.107
	opposite-side	33.8	5.9	2.106
K^+	same-side	35.6	5.3	2.110
	opposite-side	33.1	5.3	2.114
Na^+	same-side	34.9	3.2	2.112
	opposite-side	30.6	3.2	2.111
Li^+	same-side	33.9	2.1	2.115
	opposite-side	29.4	2.1	2.114

[a] Electronic energies computed at ZORA-BLYP-D3(BJ)/TZ2P. [b] The average bond length of the two newly forming C···C bonds between **bz**-$\mathbf{M^+}$ and **yne**.

Results and discussion

Alkali Cation-Benzene Complexation

First, we have analyzed the nature and strength of the interaction between benzene, **bz**, and the alkali cation, $\mathbf{M^+}$, in the initial **bz**-$\mathbf{M^+}$ reactant using the activation strain and energy decomposition analysis methods (Table 1).[13,14] The complexation energies are exclusively determined by the interaction energies, which are stabilizing and become more so when moving up Group 1, ranging from −13.1 to −38.2 kcal mol^{-1} along Cs^+ to Li^+. The trend in complexation energies follows the trend in alkali metal cation affinities (AMCA) computed by Boughlala *et al.*[27] The corresponding **bz**···$\mathbf{M^+}$ distance becomes systematically shorter from Cs^+ to Li^+, in line with the decreasing effective size of the alkali metal cation up Group 1. The orbital interactions are the major contributor to the strong **bz**···$\mathbf{M^+}$ interaction. In the case of Cs^+, they are of comparable magnitude as the electrostatic attraction. However, along Cs^+ to Li^+, the orbital interactions become relatively more important and are by far dominant in the case of lithium. The trend in orbital interactions can be rationalized upon analysis of the overlap and the orbital energy gap between the fragment molecular orbitals (FMOs) of both fragments.[28] Formation of the **bz**···$\mathbf{M^+}$ involves a key orbital interaction between the filled all-in-phase π orbital of **bz** with the empty *ns* orbital of $\mathbf{M^+}$, which increases from 0.17 for Cs^+ to 0.32 for Li^+, due to the somewhat more compact nature of the empty *ns* orbital of $\mathbf{M^+}$ when going from Cs^+ to Li^+.[27] Additionally, the drop in energy of the empty alkali cation *ns* AO, if we go up Group 1, reduces the π_{bz}-ns_{M+} orbital-energy gap,[27] which further contributes to a more stabilizing orbital interaction in the case of lighter alkali-metal cations.

Opposite-Side vs. Same-Side Reaction Pathway

Table 2 summarizes the electronic reaction barriers ($\Delta E^{\ddagger}$) and reaction energies (ΔE_{rxn}) of the uncatalyzed and alkali cation-catalyzed aromatic Diels-Alder (DA) reaction between **bz** and **yne**. Three clear trends can be observed. In the first place, the alkali cation-catalyzed DA reaction can proceed via two distinct reaction pathways, namely, opposite-side and same-side attack (Scheme 1), of which, for all alkali cations, the opposite-side DA reaction occurs with a 2–4 kcal mol^{-1} lower reaction barrier than the same-side reaction. Secondly, the coordination of an alkali cation catalyst results in a reaction barrier that systematically decreases when $\mathbf{M^+}$ goes up in Group 1. The only exception, however, is the Rb^+-catalyzed same-side DA reaction, which has a *slightly* higher barrier than the Cs^+ analog. Thirdly, the formation of all cycloadducts is endothermic, and this endothermicity decreases from the Cs^+-catalyzed to the uncatalyzed reaction and then further decreases as we climb Group 1 along $\mathbf{M^+} = Cs^+$ to Li^+.

Next, we turn to the activation strain model (ASM) of reactivity[13] to gain quantitative insight into the physical factors leading to the lower activation barrier of the opposite-side compared to same-side alkali cation-catalyzed aromatic DA reaction. In Figure 1, we focus on the activation strain diagram of the Li^+-catalyzed DA for which the catalytic effects are the

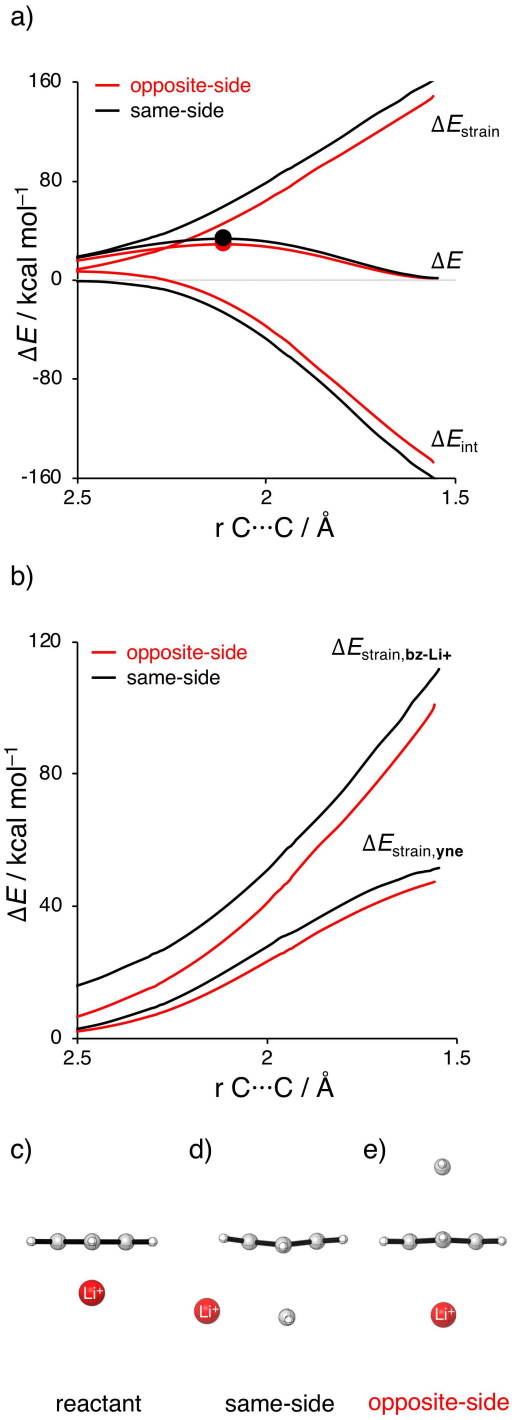

Figure 1. (a) Activation strain analysis and (b) strain decomposition analysis of the same-side and opposite-side Li^+-catalyzed aromatic Diels-Alder reaction between **bz-Li$^+$** and **yne** (TS indicated with a dot), and geometries of: (c) the reactant **bz-Li$^+$** and the reactant complexes of (d) the same-side and (e) the opposite-side pathway.

largest. The activation strain diagrams of all other alkali cation-catalyzed DA reactions possess the same, only less pronounced characteristics (Figures S1–S4 in the Supporting Information). The lower activation barrier of the opposite-side attack originates solely from a less destabilizing total strain energy. Note that the interaction energy shows a reversed trend, overruled by the trend in strain, namely, the same-side attack goes with a more stabilizing interaction energy than the opposite-side attack. The stabilizing interaction in the same-side approach stems from the direct contact between the incoming **yne** and the alkali cation. In order to determine the origin of the higher strain energy for the same-side pathway, we have decomposed this term into the strain energies of the separate reactants according to Equation (2) (Figure 1b). The more destabilizing total strain energy of the same-side attack is predominantly caused by the initial deformation of the reactant **bz-Li$^+$** in the early stage of the DA reaction. When **yne** attacks from the same-side, mutual hindrance occurs and, to avoid a rise in Pauli repulsion, the Li^+ ion moves, away from its equilibrium η^6-coordination to **bz** (Figure 1c) towards a less favorable η^2-coordination mode (Figure 1d). This deformation of the reactant **bz-Li$^+$** results in a more destabilizing $\Delta E_{\text{strain,bz-Li+}}$ compared to the opposite-side attack, where Li^+ can remain unhindered in its favorable η^6-coordination mode to **bz** in the reactant complex (Figure 1e). The, as such favorable, interaction between Li^+ and **yne** during same-side attack also induces a deformation of the reactant **yne**, leading to a further increase in destabilizing total strain energy. We also investigated the other scenario where **M$^+$** is coordinated to **yne**. We found, in line with a combined experimental and theoretical study,[29] that the bond energy associated with the formation of **yne-M$^+$** is, for all alkali cations, significantly weaker than for the formation of **bz-M$^+$** (Table S1). Therefore, if **yne-M$^+$** were to form, which is possible but not favored energetically, and the complex approaches **bz** to react, **yne-M$^+$** would bind to **bz** via **M$^+$**, which, in turn, would result in the same-side Diels-Alder reaction. This reaction pathway, as prior discussed, goes with a higher activation barrier than for the opposite-side reaction pathway.

Effect of Alkali Cations on Diels-Alder Reactivity

After having established that the alkali cation-catalyzed aromatic DA reaction of **bz-M$^+$** + **yne** proceeds preferentially via the opposite-side pathway, we have analyzed the reactivity trend of this mechanism for all five alkali cations (**M$^+$** = Li^+–Cs^+) and for the uncatalyzed reaction (**M$^+$** = none). As shown in Table 2, all transition states are located around the same average newly forming C···C bonds between **bz-M$^+$** and **yne**. Therefore, analysis of the complete potential energy surface along a reaction coordinate is not necessary. Instead, we can focus on energy terms computed at consistent geometries in the saddle-point region of the PES, all with an average C···C bond length of 2.110 Å (Table 3; see Figures S5 and S6 for complete potential energy surfaces). The trend in consistent energies, ΔE^*, in Table 3 follows that of the actual reaction barriers $\Delta E^{\ddagger}$ of Table 2, namely, the uncatalyzed reaction goes with the highest energy, introduction of a Cs^+ ion lowers the barrier which then further drops monotonically along Rb^+, K^+, Na^+, and Li^+. The acceleration of the alkali cation-catalyzed reactions originates exclusively from a more stabilizing inter-

Table 3. Activation strain and energy decomposition analyses (in [kcal mol^{-1}]) of the uncatalyzed and opposite-side catalyzed aromatic Diels-Alder reactions between **bz-M$^+$** and **yne**.[a]

M$^+$	ΔE^*	ΔE_{strain}	ΔE_{int}	ΔV_{elstat}	ΔE_{Pauli}	ΔE_{oi}	ΔE_{disp}
none	37.0	48.6	−11.6	−63.6	138.0	−77.9	−8.0
Cs$^+$	34.3	46.8	−12.5	−61.8	133.3	−76.4	−7.5
Rb$^+$	33.6	47.4	−13.8	−62.3	133.1	−77.6	−7.1
K$^+$	32.8	46.4	−13.5	−61.4	132.1	−76.8	−7.4
Na$^+$	30.4	46.7	−16.4	−61.5	131.9	−78.6	−8.1
Li$^+$	28.9	46.4	−17.5	−60.9	130.3	−78.7	−8.1

[a] Analyses at consistent TS-like geometries, all with an average C···C bond-forming distance of 2.110 Å, computed at ZORA-BLYP-D3(BJ)/TZ2P level.

action energy. The interaction energy becomes increasingly more stabilizing going from **M$^+$** = none to Cs$^+$ to Li$^+$, which determines the trend in the barrier. There is one exception, however, the interaction energy of the Rb$^+$-catalyzed reaction is *slightly* more stabilizing than the K$^+$ analog. The strain energy does not follow a clear trend, except that the strain energy for the uncatalyzed DA reaction is more destabilizing than the catalyzed analogs.

Since the interaction energy controls the observed trend in reactivity, the different contributors to the interaction energy were analyzed by applying our canonical energy decomposition analysis (EDA),[14] which quantifies the various features of the bonding mechanism (Table 3). In sharp contrast with the commonly accepted view that Lewis acids enhance the electrostatic and orbital interactions,[5] we find instead that they catalyze aromatic DA reactions solely by reducing the destabilizing Pauli repulsion. This reduced Pauli repulsion reinforces the overall stabilizing interaction between dienophile and aromatic diene and thus lowers the barrier. Furthermore, the small discrepancy in the trend in interaction energy, when going from Rb$^+$ to K$^+$ can be ascribed to both a more stabilizing ΔV_{elstat} and, as we will discuss later, a stronger normal electron demand interaction, which, in turn, yields a more stabilizing ΔE_{oi}.

To understand the origin of the less destabilizing Pauli repulsion for the alkali cation-catalyzed reactions, we performed a Kohn-Sham molecular orbital (KS-MO) analysis.[14b,28] We have quantified the two-center four-electron interactions between the filled molecular orbitals that determine the trend in Pauli repulsion between **bz-M$^+$** with **yne** in consistent geometries, close to the TS but all at the same point along the reaction coordinate, with an average C···C bond length of 2.110 Å (Figure 2a).[28] The σ-HOMO$_{bz\text{-}M+}$ has two occupied-occupied orbital interactions that are decisive for the trend in Pauli repulsion, namely, with the π-HOMO$_{yne}$ and σ-HOMO-2$_{yne}$. The respective overlap integrals and repulsion are the largest and most destabilizing for the uncatalyzed reaction (S = 0.10 and 0.07) and the smallest and least destabilizing for the Li$^+$-catalyzed reaction (S = 0.04 and 0.03). Coordination of an alkali cation to **bz** polarizes the σ-orbital of **bz** towards the alkali cation and away from the opposite-side, leading to a decreased overlap with the filled orbitals of the attacking **yne**. The donor-acceptor interactions between the empty atomic orbitals of the alkali cation, as discussed above during the analysis of the **bz···M$^+$** complexation, cause a charge transfer from **bz** to the alkali cation and result in less σ-orbital amplitude at the external σ-face of **bz** that points in the direction of the approaching **yne**. Upon going up Group 1, the extent of charge

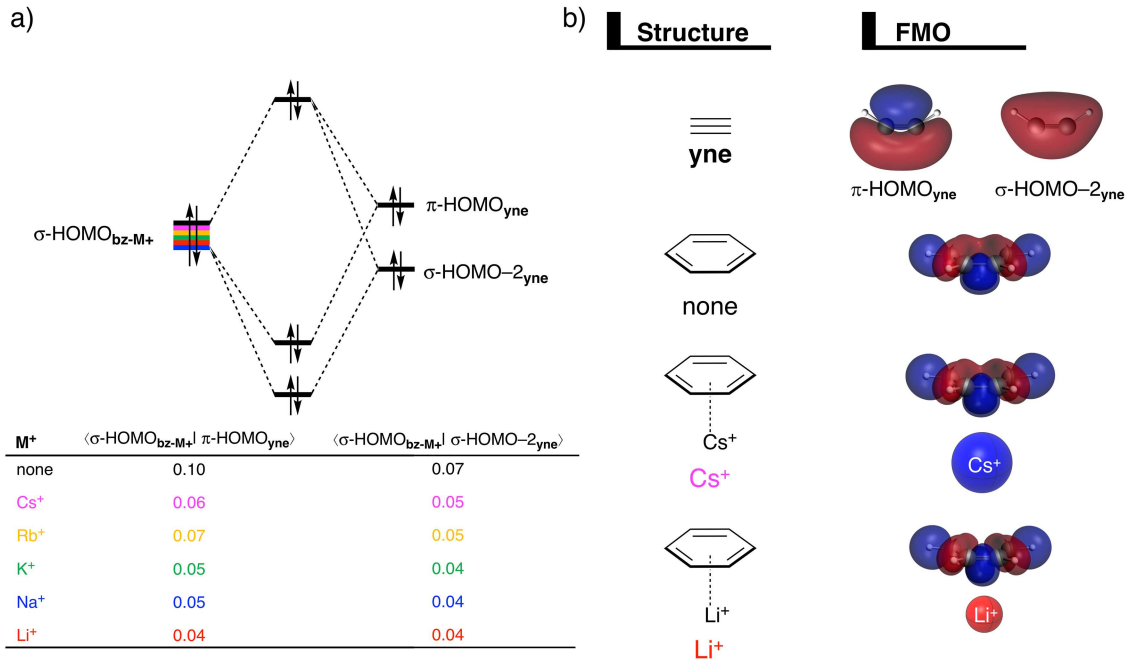

M$^+$	⟨σ-HOMO$_{bz\text{-}M+}$| π-HOMO$_{yne}$⟩	⟨σ-HOMO$_{bz\text{-}M+}$| σ-HOMO–2$_{yne}$⟩
none	0.10	0.07
Cs$^+$	0.06	0.05
Rb$^+$	0.07	0.05
K$^+$	0.05	0.04
Na$^+$	0.05	0.04
Li$^+$	0.04	0.04

Figure 2. (a) Molecular orbital diagram of the most important occupied-occupied orbital overlaps of the uncatalyzed and catalyzed opposite-side aromatic Diels-Alder reactions between **bz-M$^+$** and **yne**; and (b) key occupied orbitals (isovalue = 0.03) computed at consistent geometries with the average C···C bond-forming distance of 2.110 Å at ZORA-BLYP-D3(BJ)/TZ2P.

transfer steadily increases (from −5.9 kcal mol^{-1} for Cs^+ to −34.3 kcal mol^{-1} for Li^+; see Table 1) and, therefore, results in a progressively larger σ-$HOMO_{bz\text{-}M+}$ orbital amplitude on the side of the attacking **yne**. This can be clearly seen when comparing the central red lobes of the corresponding **bz-M$^+$** σ-densities in Figure 2b. We have previously observed this exact phenomenon in our analysis of Lewis acid-catalyzed Michael addition and Diels-Alder reactions, in which the Lewis-acid catalyst diminished the Pauli repulsion by polarizing the filled π-orbitals on the C=C double bond of the Michael acceptor or dienophile away from the filled orbitals of the attacking nucleophile or diene.[6]

Finally, we address why the current rationale behind Lewis acid-catalyzed aromatic DA reaction is incorrect, i.e., why the strength of the orbital interactions between **bz-M$^+$** and **yne** remain nearly constant upon introducing a Lewis-acidic alkali cation as catalyst (Table 3). In fact, coordination of a Lewis acidic alkali cation does strengthen the inverse electron demand (IED) interaction, between π-$LUMO_{bz\text{-}M+}$ and π-$HOMO_{yne}$ but, simultaneously, it weakens the normal electron demand (NED) interaction, between π-$HOMO_{bz\text{-}M+}$ and π-$LUMO_{yne}$. These effects cancel each other and, therefore, do not affect the overall orbital interactions between **bz-M$^+$** and **yne**. In line with the original rationale behind Lewis acid-catalyzed DA reactions, the π-$LUMO_{bz\text{-}M+}$ also gets stabilized when an alkali cation is coordinated to **bz** from −2.1 eV for the uncatalyzed to −5.9 eV for the Cs^+-catalyzed to −6.8 eV for the Li^+-catalyzed reaction, reducing the $LUMO_{bz\text{-}M+}$–$HOMO_{yne}$ gap and enhancing the IED interaction (Figure 3a).[5] However, coordination of an alkali cation stabilizes all **bz-M$^+$** orbitals, thus also the π-$HOMO_{bz\text{-}M+}$ orbital from −5.6 eV for the uncatalyzed to −9.5 eV for the Cs^+-catalyzed to −10.1 eV for the Li^+-catalyzed reaction, resulting in a larger $HOMO_{bz\text{-}M+}$–$LUMO_{yne}$ gap and weakening the NED interaction (Figure 3b).

Note that the NED orbital-energy gap of the Rb^+-catalyzed reaction is smaller than for the K^+ analog, which explains the more stabilizing ΔE_{oi} of the former, as shown in Table 3. The corresponding NED and IED orbital overlaps remain constant upon adding, or varying, the catalyzing alkali cation, which indicates that the shape of π-$HOMO_{bz\text{-}M+}$ and π-$LUMO_{bz\text{-}M+}$ orbitals do not get affected dramatically by the alkali cation because, due to a symmetry mismatch, the π-HOMO and π-LUMO orbitals of benzene have no overlap with the alkali cation *ns* acceptor AO.

Effect of Geometrical Predistortion and Heteroatoms

Next, we wish to combine the concept of Lewis acid-induced lowering of Pauli repulsion with other concepts for accelerating aromatic DA reactions in order to go for a record-low barrier. Thus, we have invoked geometrical predistortion of, and the introduction of heteroatoms in the aromatic ring as studied, amongst others,[30] by Narsaria *et al.*[4b] In their seminal work, they have shown that by using [5]metacyclophane (**m-bz**), in which the benzene core is structurally distorted by a pentamethylene bridge, instead of **bz** as the aromatic diene, the reaction barrier could be lowered by more than 20 kcal mol^{-1}, due to a reduction of strain corresponding to the aromatic diene together with an enhanced interaction with **yne** through a lowering of the HOMO–LUMO energy gap.[4b] They, additionally, substituted the C4 and C6 atoms of **m-bz** for two nitrogen atoms (**m-bz$_{(2N)}$**) which, in turn, reduced the Pauli repulsion with the incoming **yne** and resulted in a reaction barrier of only 9.7 kcal mol^{-1}, that is, 27.5 kcal mol^{-1} lower than for **bz** (Figure 4).

Thus, we have analyzed and compared the aromatic DA reactivity of **yne** with **bz**, **m-bz** and **m-bz$_{(2N)}$** with those of the

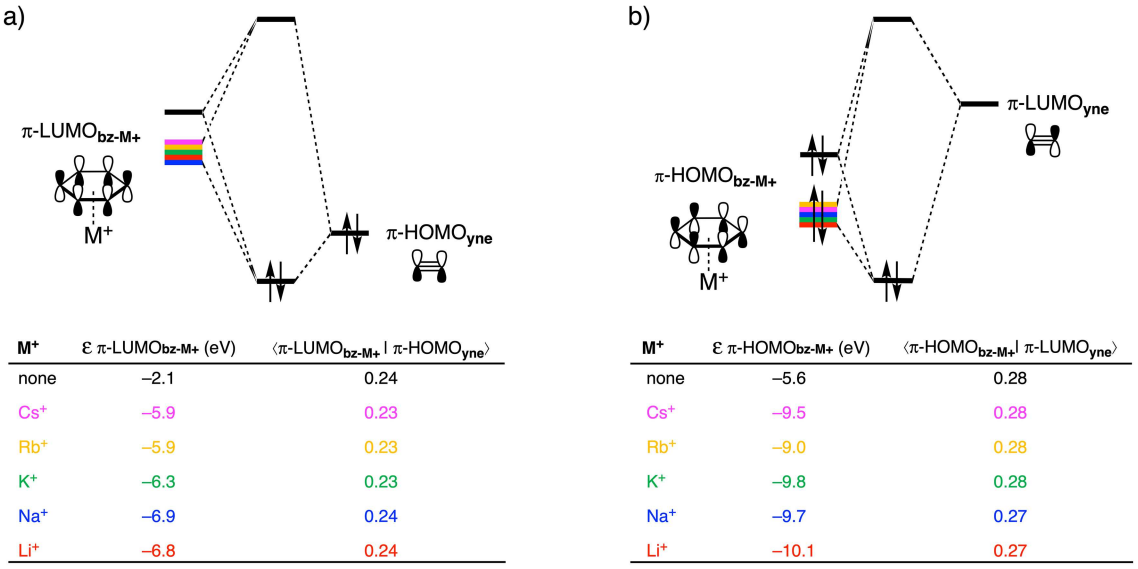

M$^+$	ε π-$LUMO_{bz\text{-}M+}$ (eV)	⟨π-$LUMO_{bz\text{-}M+}$ | π-$HOMO_{yne}$⟩
none	−2.1	0.24
Cs^+	−5.9	0.23
Rb^+	−5.9	0.23
K^+	−6.3	0.23
Na^+	−6.9	0.24
Li^+	−6.8	0.24

M$^+$	ε π-$HOMO_{bz\text{-}M+}$ (eV)	⟨π-$HOMO_{bz\text{-}M+}$| π-$LUMO_{yne}$⟩
none	−5.6	0.28
Cs^+	−9.5	0.28
Rb^+	−9.0	0.28
K^+	−9.8	0.28
Na^+	−9.7	0.27
Li^+	−10.1	0.27

Figure 3. Molecular orbital diagrams with orbital energies and overlaps: (a) for inverse electron demand π-$LUMO_{bz\text{-}M+}$–π-$HOMO_{yne}$ interactions; and (b) for normal electron demand π-$HOMO_{bz\text{-}M+}$–π-$LUMO_{yne}$ interactions of uncatalyzed and alkali cation-catalyzed opposite-side aromatic Diels-Alder reactions between **bz-M$^+$** and **yne**, computed at consistent geometries with the average C···C bond-forming distance of 2.110 Å at ZORA-BLYP-D3(BJ)/TZ2P.

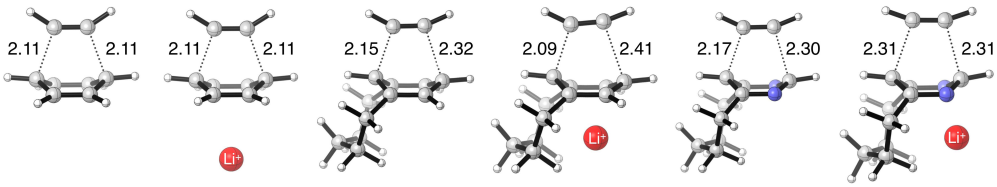

	bz	bz-Li$^+$	m-bz	m-bz-Li$^+$	m-bz$_{(2N)}$	m-bz$_{(2N)}$-Li$^+$
$\Delta E^{\ddagger}$	37.2	29.4	16.7	10.7	9.7	0.0
k_{rel}	1.0	5.2 x 10^5	1.1 x 10^{15}	2.7 x 10^{19}	1.4 x 10^{20}	2.0 x 10^{27}
ΔE_{rxn}	7.0	2.1	–27.6	–31.6	–37.1	–53.7

Figure 4. Transition state structures with forming C···C bond lengths (in Å), reaction barrier $\Delta E^{\ddagger}$ (blue; in kcal mol^{-1}), relative rate constants k_{rel} (black), and reaction energies (red; in kcal mol^{-1}) for the aromatic Diels-Alder reactions of **bz**, **bz-Li$^+$**, **m-bz**,[a] **m-bz-Li$^+$**, **m-bz$_{(2N)}$**,[a] and **m-bz$_{(2N)}$-Li$^+$** with **yne**, computed at ZORA-BLYP-D3(BJ)/TZ2P. [a] Data taken from ref [4b].

Li$^+$-catalyzed analogs **bz-Li$^+$**, **m-bz-Li$^+$** and **m-bz$_{(2N)}$-Li$^+$**. The reactions of **bz**, **bz-Li$^+$** and **m-bz$_{(2N)}$-Li$^+$** proceed via concerted synchronous transition states, whereas that of **m-bz**, **m-bz-Li$^+$**, and **m-bz$_{(2N)}$** are concerted asynchronous (Figure 4). The DA reaction barrier is reduced by 27 kcal mol^{-1} when going from **bz** to **m-bz-Li$^+$**, thereby enhancing the computed rate by 19 orders of magnitude. Strikingly, by also substituting the C4 and C6 atoms of **m-bz-Li$^+$** each by a nitrogen atom, the reaction barrier is lowered by an extra 10 kcal mol^{-1} and thus vanishes ($\Delta E^{\ddagger} = 0.0$ kcal mol^{-1}), leaving us with a spontaneous aromatic DA reaction. Note that meanwhile, the reaction energy goes from endothermic for **bz** ($\Delta E_{rxn} = 7.0$ kcal mol^{-1}) to highly exothermic for **m-bz$_{(2N)}$-Li$^+$** ($\Delta E_{rxn} = -53.7$ kcal mol^{-1}). For a detailed analysis of the reaction barriers, we refer the reader to Figures S7 and S8, Table S1, and the accompanied explanation in the Supporting Information.

Conclusion

Alkali cations (**M$^+$**) efficiently catalyze the [4 + 2] aromatic Diels-Alder (DA) reaction between benzene (**bz**) and acetylene (**yne**) by coordinating to the aromatic diene. The pathway in which **yne** and **M$^+$** are on opposite sides of **bz** ("opposite-side" reaction) goes, for all alkali cations, with a lower barrier than the pathway in which **yne** and **M$^+$** are on the same side of **bz** ("same-side" reaction), where they hinder each other in early stages of the reaction. The catalytic effect is stronger for lighter alkali cations, that is, the aromatic DA reaction barrier decreases along **M$^+$** = none > Cs$^+$ > Rb$^+$ > K$^+$ > Na$^+$ > Li$^+$.

Strikingly and in contrast to widespread belief, the enhanced reactivity of the alkali cation-catalyzed, compared to the uncatalyzed, aromatic DA reaction is solely caused by reduced Pauli repulsion between the reactants **bz-M$^+$** and **yne** and, not by enhanced stabilizing orbital interactions. The reason for the reduced Pauli repulsion is that the alkali cation in **bz-M$^+$** polarizes orbitals of benzene away from the opposite side at which the **yne** attacks, resulting in less occupied-occupied orbital overlap. This polarization effect induced by the alkali cation becomes more pronounced as we move up Group 1, because the lighter alkali cations, with lower-energy valence *s* AOs, enter into a stronger donor-acceptor interaction with the occupied orbitals of **bz**.

The aforementioned result that the stabilizing orbital interactions remain essentially unchanged upon, and are, therefore, not responsible for, alkali-cation catalysis is possibly as surprising as the insight that the reduced Pauli repulsion is the key causal mechanism behind the catalytic effect. This invariability of the orbital interactions appears to be the result of two counteracting effects that offset each other: Coordination of an alkali cation to **bz** stabilizes all the **bz-M$^+$** orbitals and, therefore, enhances the inverse electron demand interaction by reducing the orbital-energy gap between empty **bz-M$^+$** π-orbitals and filled **yne** π-orbitals while it simultaneously weakens the normal electron demand interaction by increasing the orbital-energy gap between filled **bz-M$^+$** π-orbitals and empty **yne** π^* orbitals.

This study demonstrates the more general applicability of a reduction of Pauli repulsion being the causal actor behind the catalytic effect of Lewis acids in organic reactions and we hope it will also be valuable for the understanding of the interstellar formation of polycyclic aromatic hydrocarbons. In a final attempt to demonstrate the predictive power of our model, we have successfully combined our present findings with the concepts of geometrical predistortion and heteroatom substitution in the aromatic ring,[4b] to push the aromatic DA reaction barrier down from 37 kcal mol^{-1} for **bz** + **yne** to a remarkable 0 kcal mol^{-1} for **m-bz$_{(2N)}$-Li$^+$** + **yne**.

Acknowledgments

We thank the Netherlands Organization for Scientific Research (NWO) and the Dutch Astrochemistry Network (DAN) for financial support. Furthermore, we thank Ayush K. Narsaria for helpful discussions on the topic of combining predistortion and alkali cation catalysis to further enhance the aromatic Diels-Alder reactivity.

Conflict of Interest

The authors declare no conflict of interest.

Keywords: Activation Strain Model · Alkali Cation · Aromatic Diels-Alder Reaction · Density Functional Calculations · Reactivity

[1] a) J. Sauer, *Angew. Chem.* **1967**, *79*, 76; *Angew. Chem. Int. Ed. Engl.* **1967**, *6*, 16; b) R. S. H. Liu, C. G. Krespan, *J. Org. Chem.* **1969**, *34*, 1271; c) J. P. N. Brewer, H. Heaney, *Tetrahedron Lett.* **1965**, *6*, 4709; d) G. Zhong, B. Chan, L. Radom, *J. Am. Chem. Soc.* **2007**, *129*, 924; e) E. Ciganek, *Tetrahedron Lett.* **1967**, *8*, 3321.
[2] a) D. Biermann, W. Schmidt, *J. Am. Chem. Soc.* **1980**, *102*, 3163; b) D. Biermann, W. Schmidt, *J. Am. Chem. Soc.* **1980**, *102*, 3173.
[3] a) U. Pindur, G. Lutz, C. Otto, *Chem. Rev.* **1993**, *93*, 741; b) F. Fringuelli, O. Piermatti, F. Pizzo, L. Vaccaro, *Eur. J. Org. Chem.* **2001**, 439.
[4] a) D. J. Cram, J. M. Cram, *Acc. Chem. Res.* **1971**, *4*, 204; b) A. K. Narsaria, T. A. Hamlin, K. Lammertsma, F. M. Bickelhaupt, *Chem. Eur. J.* **2019**, *25*, 9902; c) O. T. Dyan, G. I. Borodkin, P. A. Zakin, *Eur. J. Org. Chem.* **2019**, 7271.
[5] I. Fleming, *Frontier Orbitals and Organic Chemical Reactions*, Wiley, New York, **1976**. New edition: I. Fleming, *Molecular Orbitals and Organic Chemical Reactions*, Wiley, New Jersey, **2009**.
[6] a) T. A. Hamlin, I. Fernández, F. M. Bickelhaupt, *Angew. Chem.* **2019**, *131*, 9015; *Angew. Chem. Int. Ed.* **2019**, *58*, 8922; b) P. Vermeeren, T. A. Hamlin, I. Fernández, F. M. Bickelhaupt, *Angew. Chem. Int. Ed.* **2020**, DOI: 10.1002/anie.2019114582.
[7] a) E. Buncel, K. G. Albright, I. Onyido, *Org. Biomol. Chem.* **2004**, *2*, 601; b) P. Gomez-Tagle, I. Vargas-Zúñiga, O. Taran, A. Yatsimirsky, *J. Org. Chem.* **2006**, *71*, 9713; c) I. H. Um, Y. H. Shin, S. E. Lee, K. Yang, E. Buncel, *J. Org. Chem.* **2008**, *73*, 923; d) I. H. Um, J. S. Kang, Y. H. Shin, E. Buncel, *J. Org. Chem.* **2012**, *78*, 490; e) I. H. Um, Y. H. Shin, J. E. Park, J. S. Kang, E. Buncel, *Chem. Eur. J.* **2012**, *18*, 961.
[8] a) E. van Lenthe, R. van Leeuwen, E. J. Baerends, J. G. Snijders, *Int. J. Quantum Chem.* **1996**, *57*, 281; b) E. van Lenthe, E. J. Baerends, J. G. Snijders, *J. Chem. Phys.* **1994**, *101*, 9783.
[9] a) A. D. Becke, *Phys. Rev. A* **1988**, *38*, 3098; b) C. T. Lee, W. T. Yang, R. G. Parr, *Phys. Rev. B* **1988**, *37*, 785; c) B. G. Johnson, P. M. W. Gill, J. A. Pople, *J. Chem. Phys.* **1993**, *98*, 5612; d) T. V. Russo, R. L. Martin, P. J. Hay, *J. Chem. Phys.* **1994**, *101*, 7729.
[10] a) S. Grimme, J. Antony, S. Ehrlich, H. Krieg, *J. Chem. Phys.* **2010**, *132*, 154104; b) S. Grimme, S. Ehrlich, L. Goerigk, *J. Comput. Chem.* **2011**, *32*, 1456.
[11] E. van Lenthe, E. J. Baerends, *J. Comput. Chem.*, **2003**, *24*, 1142.
[12] a) ADF2017, SCM, Theoretical Chemistry, Vrije Universiteit, Amsterdam (The Netherlands), **2017**; b) G. te Velde, F. M. Bickelhaupt, E. J. Baerends, C. Fonseca Guerra, S. J. A. van Gisbergen, J. G. Snijders, T. Ziegler, *J. Comput. Chem.* **2001**, *22*, 931; c) C. Fonseca Guerra, J. G. Snijders, G. te Velde, E. J. Baerends, *Theor. Chem. Acc.* **1998**, *99*, 391.
[13] For a step-by-step protocol, see: a) P. Vermeeren, S. C. C. van der Lubbe, C. Fonseca Guerra, F. M. Bickelhaupt, T. A. Hamlin, *Nat. Protoc.* **2020**, *15*, 649; for reviews, see: b) F. M. Bickelhaupt, *J. Comput. Chem.* **1999**, *20*, 114; c) W.-J. van Zeist, F. M. Bickelhaupt, *Org. Biomol. Chem.* **2010**, *8*, 3118; d) I. Fernández, F. M. Bickelhaupt, *Chem. Soc. Rev.* **2014**, *43*, 4953; e) L. P. Wolters, F. M. Bickelhaupt, *WIREs Comput. Mol. Sci.* **2015**, *5*, 324; f) F. M. Bickelhaupt, K. N. Houk, *Angew. Chem.* **2017**, *129*, 10204; *Angew. Chem. Int. Ed.* **2017**, *56*, 10070.
[14] a) F. M. Bickelhaupt, E. J. Baerends, in *Reviews in Computational Chemistry* (Eds.: K. B. Lipkowitz, D. B. Boyd), Wiley, Hoboken, **2000**, pp. 1–86; b) R. van Meer, O. V. Gritsenko, E. J. Baerends, *J. Chem. Theory Comput.* **2014**, *10*, 4432.
[15] a) P. Ehrenfreund, M. A. Sephton, *Faraday Discuss.* **2006**, *133*, 277; b) A. G. G. M. Tielens, *Annu. Rev. Astron. Astrophys.* **2008**, *46*, 286; c) E. Herbst, E. F. van Dishoeck, *Annu. Rev. Astron. Astrophys.* **2009**, *47*, 427; d) A. G. G. M. Tielens, *Rev. Mod. Phys.* **2013**, *85*, 1021.
[16] a) L. J. Allamandola, S. A. Sandford, B. Wopenka, *Science* **1987**, *237*, 56; b) W. M. Irvine, *Origins Life Evol. Biospheres* **1998**, *28*, 365; P. Ehrenfreund, S. B. Charnley, *Annu. Rev. Astron. Astrophys.* **2000**, *38*, 427.
[17] a) H. E. Zimmerman, G. L. Grunewald, *J. Am. Chem. Soc.* **1964**, *86*, 1434; b) E. T. Akin, M. Erdogan, A. Dastan, N. Saracoglu, *Tetrahedron* **2017**, *73*, 5537.
[18] a) F. Tera, O. Eugster, D. S. Burnett, G. J. Wasserburg, *Geochim. Cosmochim. Acta* **1970**, *1*, 1637; b) J. Cernicharo, M. Guélin, *Astron. Astrophys.* **1987**, *183*, L10; c) G. Edwards, H. C. Urey, *Geochim. Cosmochim. Acta* **1970**, *7*, 154; d) P. W. Gast, *Geochim. Cosmochim. Acta* **1960**, *19*, 1; e) K. S. Heier, J. A. Adams, *PHYS. CHEM. EARTH* **1964**, *5*, 253; f) B. E. Turner, T. C. Steimle, L. Meerts, *Astrophys. J.* **1994**, *426*, 97.
[19] T. A. Hamlin, D. Svatunek, S. Yu, L. Ridder, I. Infante, L. Visscher, F. M. Bickelhaupt, *Eur. J. Org. Chem.* **2019**, 378.
[20] a) M. Franchini, P. H. T. Philipsen, E. van Lenthe, L. Visscher, *J. Chem. Theory Comput.* **2014**, *10*, 1994; b) M. Franchini, P. H. T. Philipsen, L. Visscher, *J. Comput. Chem.* **2013**, *34*, 1819.
[21] a) A. Bérces, R. M. Dickson, L. Fan, H. Jacobsen, D. Swerhone, T. Ziegler, *Comput. Phys. Commun.* **1997**, *100*, 247; b) H. Jacobsen, A. Bérces, D. P. Swerhone, T. Ziegler, *Comput. Phys. Commun.* **1997**, *100*, 263; c) S. K. Wolff, *Int. J. Quantum Chem.* **2005**, *104*, 645.
[22] a) K. Fukui, *Acc. Chem. Res.* **1981**, *14*, 363; b) L. Deng, T. Ziegler, L. Fan, *J. Chem. Phys.* **1993**, *99*, 3823; c) L. Deng, T. Ziegler, *Int. J. Quantum Chem.* **1994**, *52*, 731.
[23] a) W. J. van Zeist, C. Fonseca Guerra, F. M. Bickelhaupt, *J. Comput. Chem.* **2008**, *29*, 312; b) X. Sun, T. M. Soini, J. Poater, T. A. Hamlin, F. M. Bickelhaupt, *J. Comput. Chem.* **2019**, *40*, 2227.
[24] C. Y. Legault, *CYLview*, Unversité de Sherbrooke, Sherbrooke, QC (Canada), **2009**.
[25] a) D. H. Ess, K. Houk, *J. Am. Chem. Soc.* **2007**, *129*, 10646; b) D. H. Ess, K. Houk, *J. Am. Chem. Soc.* **2008**, *130*, 10187.
[26] See, for instance: a) P. Vermeeren, X. Sun, F. M. Bickelhaupt, *Sci. Rep.* **2018**, *8*, 10729; b) X. Sun, M. V. J. Rocha, T. A. Hamlin, J. Poater, F. M. Bickelhaupt, *Phys. Chem. Chem. Phys.* **2019**, *21*, 9651; c) S. Yu, H. M. de Bruijn, D. Svatunek, T. A. Hamlin, F. M. Bickelhaupt, *ChemistryOpen* **2018**, *7*, 995.
[27] Z. Boughlala, C. Fonseca Guerra, F. M. Bickelhaupt, *Chem. Asian J.* **2017**, *12*, 2604.
[28] T. A. Albright, J. K. Burdett, W. H. Wangbo, *Orbital Interactions in Chemistry*, Wiley, New York, **2013**.
[29] D. V. Moreno, S. A. Gonzálezm A Reyes, *J. Phys. Chem. A* **2010**, *114*, 9231.
[30] See, for instance: a) D. L. Boger, *Chem. Rev.* **1986**, *86*, 781; b) A. J. Ashe, M. D. Gordon, *J. Am. Chem. Soc.* **1972**, *94*, 7596; c) D. J. Cram, J. M. Cram, *Acc. Chem. Res.* **1971**, *4*, 204; d) M. J. van Eis, C. M. D. Komen, F. J. J. de Kanter, W. H. de Wolf, K. Lammertsma, F. Bickelhaupt, M. Lutz, A. L. Spek, *Angew. Chem.* **1998**, *110*, 1656; *Angew. Chem. Int. Ed.* **1998**, *37*, 1547.

Manuscript received: January 3, 2020
Revised manuscript received: January 24, 2020
Accepted manuscript online: February 3, 2020
Version of record online: March 9, 2020